Sfermion pair production at $\mu^+\mu^-$ colliders

A. Bartl and W. Porod*
Institut für Theoretische Physik, Universität Wien, A-1090 Vienna, Austria

H. Eberl, S. Kraml, and W. Majerotto
Institut für Hochenergiephysik der Österreichischen Akademie der Wissenschaften, A-1050 Vienna, Austria
(Received 11 May 1998; published 13 October 1998)

We discuss pair production of top squarks, sbottoms, staus, and tau sneutrinos at a $\mu^+\mu^-$ collider. We present the formulas for the production cross sections and perform a detailed numerical analysis within the minimal supersymmetric standard model. In particular, we consider sfermion production near $\sqrt{s}=m_{H^0}$ and $\sqrt{s}=m_{A^0}$. [S0556-2821(98)09519-8]

PACS number(s): 14.80.Ly, 12.60.Jv, 14.80.Cp

I. INTRODUCTION

The search for supersymmetry (SUSY) [1,2] is one of the main issues in the experimental programs at the CERN e^+e^- collider LEP2 and Fermilab Tevatron. It will play an even more important role at the future Large Hadron Collider (LHC), e^+e^- linear colliders with an energy range up to 2 TeV, and $\mu^+\mu^-$ colliders with an energy range up to 4 TeV. The Tevatron and LHC are well designed to discover SUSY. At these machines even some precision measurements are possible [3]. However, for a precise determination of the underlying SUSY parameters lepton colliders will be necessary. Owing to their good energy resolution, $\mu^+\mu^-$ colliders are well suited for this purpose [4,5]. The most exciting feature is the possibility of producing Higgs bosons in the s channel [4–6].

In this paper we study the production of third generation sfermions in $\mu^+\mu^-$ annihilation, paying particular attention to the energy range near the Higgs boson resonances. Our framework is the minimal supersymmetric standard model (MSSM) [2,7]. The MSSM implies the existence of five physical Higgs bosons: two scalars h^0, H^0, one pseudoscalar A^0, and two charged ones $H^\pm$ [7,8]. Every standard model (SM) fermion has two supersymmetric partners, one for each chirality state denoted by $\tilde{f}_L$ and $\tilde{f}_R$.

The sfermions of the third generation are particularly interesting [9–11] because their phenomenology is different compared to that of the sfermions of the first and second generation. The reasons for this are the mixing between $\tilde{f}_L$ and $\tilde{f}_R$ and the large Yukawa couplings.

In particular, the top quark and the top squarks give substantial contributions to Higgs boson masses due to radiative corrections (see, e.g., [12,13]). Moreover, the top quark and top squark contributions to the renormalization group equations play an essential role in inducing electroweak symmetry breaking, when the Higgs parameters evolve from the grand unified theory (GUT) scale to the electroweak scale [14]. Therefore, the couplings of the top squarks to the neutral Higgs bosons are of special interest. Also the tau and bottom Yukawa couplings can be large if $\tan\beta$ is large, giving rise to similar effects in the phenomenology of sbottoms and staus.

The paper is organized in the following way: In Sec. II we present the underlying parameters and give the formulas for the production cross sections. In Sec. III we discuss numerical results for sfermion pair production. In Sec. IV we summarize the main results. In the Appendix we give the Higgs sfermion couplings.

II. SFERMION PAIR PRODUCTION

In this section we present the formulas for sfermion mixing and the production cross sections of sfermions at a $\mu^+\mu^-$ collider. The main parameters for the following discussion are $m_{A^0}, \mu, \tan\beta, M_{\tilde{D}}, M_{\tilde{Q}}, M_{\tilde{U}}, M_{\tilde{E}}, M_{\tilde{L}}, A_b, A_t$, and A_τ [2,7]. m_{A^0} is the mass of the pseudoscalar Higgs boson, μ is the Higgs mixing parameter in the superpotential, and $\tan\beta=v_2/v_1$, where v_i denotes the vacuum expectation value of the Higgs doublet H_i. $M_{\tilde{D}}, M_{\tilde{Q}}, M_{\tilde{U}}, M_{\tilde{E}}$ and $M_{\tilde{L}}$ are soft SUSY breaking masses for the sfermions, A_b, A_t, and A_τ are trilinear Higgs-sfermion parameters.

The mass matrix for sfermions in the $(\tilde{f}_L, \tilde{f}_R)$ basis has the following form:

$$\mathcal{M}^2_{\tilde{f}} = \begin{pmatrix} m^2_{\tilde{f}_L} & a_f m_f \\ a_f m_f & m^2_{\tilde{f}_R} \end{pmatrix} \tag{1}$$

with

$$m^2_{\tilde{t}_L} = M^2_{\tilde{Q}} + m_t^2 + m_Z^2 \cos 2\beta \left(\tfrac{1}{2} - \tfrac{2}{3}\sin^2\theta_W\right),$$

$$m^2_{\tilde{t}_R} = M^2_{\tilde{U}} + m_t^2 + \tfrac{2}{3} m_Z^2 \cos 2\beta \sin^2\theta_W,$$

$$m^2_{\tilde{b}_L} = M^2_{\tilde{Q}} + m_b^2 - m_Z^2 \cos 2\beta \left(\tfrac{1}{2} - \tfrac{1}{3}\sin^2\theta_W\right),$$

$$m^2_{\tilde{b}_R} = M^2_{\tilde{D}} + m_b^2 - \tfrac{1}{3} m_Z^2 \cos 2\beta \sin^2\theta_W,$$

*Present address: Instituto de Física Corpuscular – IFIC/CISC, Departament de Física Teórica, E-46100 Burjassot, Válencia, Spain.

$$m^2_{\tilde{\tau}_L} = M^2_{\tilde{L}} + m^2_\tau - m^2_Z \cos 2\beta \left(\tfrac{1}{2} - \sin^2\theta_W\right),$$

$$m^2_{\tilde{\tau}_R} = M^2_{\tilde{E}} + m^2_\tau - m^2_Z \cos 2\beta \sin^2\theta_W, \tag{2}$$

and

$$a_t = A_t - \mu \cot\beta,$$

$$a_b = A_b - \mu \tan\beta,$$

$$a_\tau = A_\tau - \mu \tan\beta. \tag{3}$$

The mass eigenstates $\tilde{f}_1$ and $\tilde{f}_2$ are related to $\tilde{f}_L$ and $\tilde{f}_R$ by:

$$\begin{pmatrix} \tilde{f}_1 \\ \tilde{f}_2 \end{pmatrix} = \begin{pmatrix} \cos\theta_{\tilde{f}} & \sin\theta_{\tilde{f}} \\ -\sin\theta_{\tilde{f}} & \cos\theta_{\tilde{f}} \end{pmatrix} \begin{pmatrix} \tilde{f}_L \\ \tilde{f}_R \end{pmatrix} \tag{4}$$

with the eigenvalues

$$m^2_{\tilde{f}_{1,2}} = \tfrac{1}{2}\left(m^2_{\tilde{f}_L} + m^2_{\tilde{f}_R}\right) \mp \tfrac{1}{2}\sqrt{\left(m^2_{\tilde{f}_L} - m^2_{\tilde{f}_R}\right)^2 + 4a_f^2 m_f^2}. \tag{5}$$

The mixing angle $\theta_{\tilde{f}}$ is given by

$$\cos\theta_{\tilde{f}} = \frac{-a_f m_f}{\sqrt{\left(m^2_{\tilde{f}_L} - m^2_{\tilde{f}_1}\right)^2 + a_f^2 m_f^2}},$$

$$\sin\theta_{\tilde{f}} = \sqrt{\frac{\left(m^2_{\tilde{f}_L} - m^2_{\tilde{f}_1}\right)^2}{\left(m^2_{\tilde{f}_L} - m^2_{\tilde{f}_1}\right)^2 + a_f^2 m_f^2}}. \tag{6}$$

The mass of the tau sneutrino is given by

$$m^2_{\tilde{\nu}_\tau} = M^2_{\tilde{L}} - \tfrac{1}{2} m^2_Z \cos 2\beta. \tag{7}$$

Figure 1 shows the Feynman graphs for the processes $\mu^+\mu^- \to \tilde{f}_i \bar{\tilde{f}}_j \, (i,j = 1,2)$. The total and the differential cross sections read up to $\mathcal{O}(m_\mu^2)$:

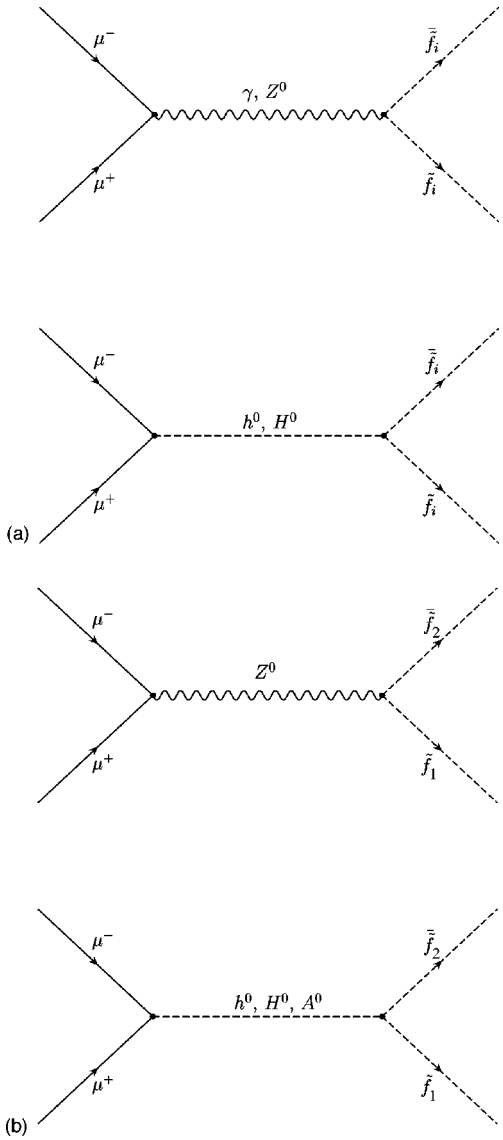

FIG. 1. Feynman graphs for sfermion production in $\mu^+\mu^-$ annihilation: (a) for $\tilde{f}_i \bar{\tilde{f}}_i \, (i = 1,2)$, (b) for $\tilde{f}_1 \bar{\tilde{f}}_2$.

$$\sigma(\mu^+\mu^- \to \tilde{f}_i \bar{\tilde{f}}_j) = c_{ij}\left(\frac{4}{3}\frac{\lambda_{ij}}{s^2} T_{VV} + 2\frac{m^2_{\tilde{f}_i} - m^2_{\tilde{f}_j}}{s} T^a_{VH} + 2T_{HH}\right), \tag{8}$$

$$\frac{d\sigma(\mu^+\mu^- \to \tilde{f}_i \bar{\tilde{f}}_j)}{d\cos\vartheta} = c_{ij}\left(\frac{\lambda_{ij}}{s^2} T_{VV} \sin^2\vartheta + \frac{m^2_{\tilde{f}_i} - m^2_{\tilde{f}_j}}{s} T^a_{VH} + \frac{\lambda_{ij}^{1/2}}{s} T^b_{VH} \cos\vartheta + T_{HH}\right) \tag{9}$$

with the kinematic function $\lambda_{ij}=(s-m_{\tilde{f}_i}^2-m_{\tilde{f}_j}^2)^2-4m_{\tilde{f}_i}^2 m_{\tilde{f}_j}^2$, ϑ the scattering angle of $\tilde{f}_i$, and

$$c_{ij}=\frac{\pi N_C \alpha^2}{4s^2}\lambda_{ij}^{1/2}, \tag{10}$$

where N_C is a color factor which is 3 for squarks and 1 for sleptons.

T_{VV} denotes the contribution from γ and Z^0 exchange, $T_{VH}^{a,b}$ the interference terms between gauge and Higgs bosons, and T_{HH} the contribution stemming from the exchange of Higgs bosons. The pure gauge boson contribution, the first term of Eqs. (8) and (9), is the same as for $e^+e^-\to\tilde{f}_i\overline{\tilde{f}_j}$ [15]. Notice that the gauge boson term shows a $\sin^2\vartheta$ dependence whereas the terms proportional to T_{HH} and T_{VH}^a are independent of ϑ. The term proportional to T_{VH}^b shows a $\cos\vartheta$ dependence giving rise to a forward–backward asymmetry. However, T_{VH}^b is proportional to m_μ (see the following equations) and, therefore, is rather small.

We obtain the following.

(1) $i=j$

$$T_{VV}=e_f^2-\frac{e_f a_{ii} v_\mu s}{8\sin^2\theta_W\cos^2\theta_W}\mathrm{Re}[D(Z)]+\frac{a_{ii}^2(v_\mu^2+a_\mu^2)s^2}{256\sin^4\theta_W\cos^4\theta_W}|D(Z)|^2,$$

$$T_{HH}=h_\mu^2\frac{s}{2e^2\sin^2\theta_W}|G_{ii}^{h^0}\sin\alpha D(h^0)-G_{ii}^{H^0}\cos\alpha D(H^0)|^2,$$

$$T_{VH}^a=0,$$

$$T_{VH}^b=h_\mu m_\mu\frac{2\sqrt{2}}{e\sin\theta_W}\Bigg(e_f\mathrm{Re}[G_{ii}^{h^0}\sin\alpha D(h^0)-G_{ii}^{H^0}\cos\alpha D(H^0)] - \frac{v_\mu a_{ii}s}{16\sin^2\theta_W\cos^2\theta_W}\mathrm{Re}[D^*(Z)(G_{ii}^{h^0}\sin\alpha D(h^0)-G_{ii}^{H^0}\cos\alpha D(H^0))]\Bigg). \tag{11}$$

(2) $i\neq j$

$$T_{VV}=\frac{a_{ij}^2(v_\mu^2+a_\mu^2)s^2}{256\sin^4\theta_W\cos^4\theta_W}|D(Z)|^2,$$

$$T_{HH}=h_\mu^2\frac{s}{2e^2\sin^2\theta_W}[|G_{ij}^{h^0}\sin\alpha D(h^0)-G_{ij}^{H^0}\cos\alpha D(H^0)|^2+|\sin\beta G_{12}^{A^0}D(A^0)|^2],$$

$$T_{VH}^a=-h_\mu m_\mu\frac{\sqrt{2}a_{ij}a_\mu\sin\beta s}{8e\sin^3\theta_W\cos^2\theta_W}G_{12}^{A^0}\mathrm{Re}[D^*(Z)D(A^0)],$$

$$T_{VH}^b=-h_\mu m_\mu\frac{\sqrt{2}v_\mu a_{ij}s}{8e\sin^4\theta_W\cos^2\theta_W}\mathrm{Re}[D^*(Z)(G_{ij}^{h^0}\sin\alpha D(h^0)-G_{ij}^{H^0}\cos\alpha D(H^0))], \tag{12}$$

where h_μ is the Yukawa coupling of the muon, $h_\mu=gm_\mu/(\sqrt{2}m_W\cos\beta)$, $D(i)=1/((s-m_i^2)+i\Gamma_i m_i)$; e_f is the charge of the sfermions ($e_t=2/3, e_b=-1/3, e_\tau=-1$) v_μ and a_μ are the vector and axial vector couplings of the muon to the Z boson, $v_\mu=-1+4\sin^2\theta_W$, $a_\mu=-1$, and a_{ij} are the corresponding couplings $Z\tilde{f}_i\overline{\tilde{f}_j}$:

$$a_{11}=4(I_f^{3L}\cos^2\theta_{\tilde{f}}-\sin^2\theta_W e_f),$$

$$a_{22}=4(I_f^{3L}\sin^2\theta_{\tilde{f}}-\sin^2\theta_W e_f),$$

$$a_{12}=a_{21}=-2I_f^{3L}\sin 2\theta_{\tilde{f}}, \tag{13}$$

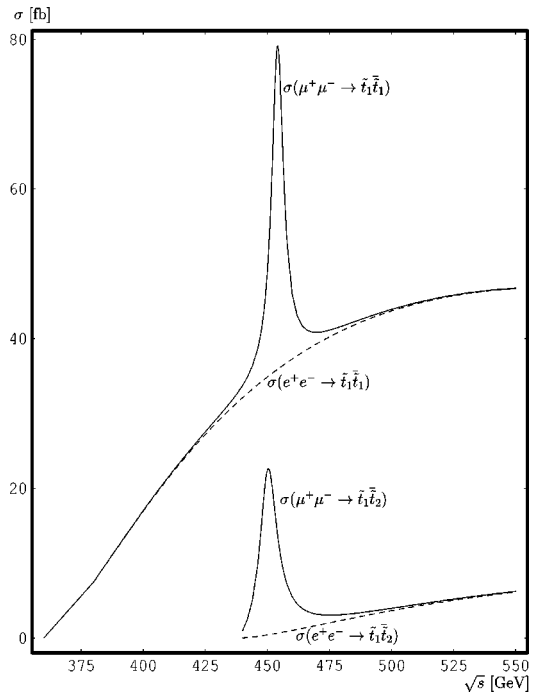

FIG. 2. Cross sections for stop production as a function of $\sqrt{s}$ for $m_{\tilde{t}_1}=180$ GeV, $m_{\tilde{t}_2}=260$ GeV, $\cos\theta_{\tilde{t}}=-0.556$, $m_{\tilde{b}_1}=175$ GeV, $m_{\tilde{b}_2}=195$ GeV, $\cos\theta_{\tilde{b}}=0.9$, $\mu=300$ GeV, $M=120$ GeV, $\tan\beta=3$, and $m_{A^0}=450$ GeV. The full lines show the cross sections at a $\mu^+\mu^-$ collider and the dashed lines the corresponding ones at an e^+e^- collider.

where I_f^{3L} is the third component of the weak isospin of the fermion f. $G_{ij}^{h^0}$, $G_{ij}^{H^0}$, and $G_{ij}^{A^0}$ are the couplings of the sfermions $\tilde{f}_i$ and $\tilde{f}_j$ (i, j =1, 2) to the light, the heavy, and the pseudoscalar Higgs boson, respectively. These couplings depend on A_f, μ, $\tan\beta$, $\cos\theta_{\tilde{f}}$, $\cos\alpha$, where α is the mixing angle of h^0 and H^0. The explicit form of these couplings is given in the Appendix.

III. NUMERICAL RESULTS

In this section we present the numerical results for sfermion production in the various channels. In this analysis we have taken: $\alpha(m_Z)=1/129$, $\sin^2\theta_W=0.23$, $m_Z=91.187$ GeV, $m_t=175$ GeV, $m_b=5$ GeV, and $m_\mu=105.66$ MeV. For the calculation of the cross section, we need the total decay widths of the Higgs bosons, where we calculate all possible two-body decay modes that are allowed at tree-level [16]. For this calculation we fix $M=120$ GeV and use the GUT relation $M'=5/3\tan^2\theta_W M$, where M and M' are the $SU(2)$ and $U(1)$ gaugino masses, respectively. As usual we have included radiative corrections in the calculation of m_{h^0}, m_{H^0}, and $\cos\alpha$ using [12].

In Fig. 2 we show the total cross sections for stop production as a function of $\sqrt{s}$ for $\mu=300$ GeV, $\tan\beta=3$, $m_{\tilde{t}_1}=180$ GeV, $m_{\tilde{t}_2}=260$ GeV, $\cos\theta_{\tilde{t}}=-0.556$, and $m_{A^0}=450$ GeV. For the total widths of the Higgs bosons, we take $m_{\tilde{b}_1}=175$ GeV, $m_{\tilde{b}_2}=195$ GeV, $\cos\theta_{\tilde{b}}=0.9$, $M_{\tilde{L}}=170$ GeV, $M_{\tilde{E}}=150$ GeV, and $A_\tau=300$ GeV. The full lines show the total cross sections and the dashed lines the gauge boson contributions. The latter ones are identical with the cross sections of $e^+e^-\to\tilde{t}_i\bar{\tilde{t}}_j$. For $\tilde{t}_1\bar{\tilde{t}}_1$ production the peak results from the H^0 exchange leading to an enhancement of ~ 40 fb compared to the gauge boson contribution. For $\tilde{t}_1\bar{\tilde{t}}_2$ production the peak is an overlap of the H^0 and A^0 resonances because $m_{A^0}\simeq m_{H^0}$ and the widths of A^0 and H^0 are of the order of several GeV (see, e.g. [8,17,18]). Note that the Higgs boson contribution is much larger than the gauge boson contribution. We have found that the forward-backward asymmetry A_{FB} is $\sim 10^{-4}$ at its maximum. Therefore, a rather high luminosity would be needed to measure it.

In Fig. 3 we show the production cross sections for $\mu^+\mu^-\to\tilde{t}_1\bar{\tilde{t}}_1$ and $\mu^+\mu^-\to\tilde{t}_1\bar{\tilde{t}}_2$ (without including the charge conjugate state) as a function of $\cos\theta_{\tilde{t}}$. We have chosen the following procedure for the calculation of the parameters: We fix $m_{\tilde{t}_1}=180$ GeV, $m_{\tilde{t}_2}=260$ GeV, $A_b=300$ GeV, and μ, $\tan\beta$, m_{A^0}, $M_{\tilde{L}}$, $M_{\tilde{E}}$, A_τ as above. We calculate $M_{\tilde{Q}}$, $M_{\tilde{U}}$, and A_t from the top squark masses and mixing angle. We take $M_{\tilde{D}}=1.12\,M_{\tilde{Q}}$ (we have checked, that our results are not sensitive to this assumption). These parameters are then used for the calculation of $m_{\tilde{b}_1}$, $m_{\tilde{b}_2}$, $\cos\theta_{\tilde{b}}$, m_{h^0}, m_{H^0}, $\cos\alpha$, Γ_{H^0}, and Γ_{A^0}. We have chosen this procedure to minimize the dependence of the physical Higgs quantities on $\cos\theta_{\tilde{t}}$. In Fig. 3a we show the total cross section $\sigma(\mu^+\mu^-\to\tilde{t}_1\bar{\tilde{t}}_1)$, the Higgs boson contribution, and the gauge boson contribution for $\sqrt{s}=453$ GeV. The Higgs boson contribution depends on the sign of $\cos\theta_{\tilde{t}}$. This leads to a dependence of the total cross section on the sign of $\cos\theta_{\tilde{t}}$ contrary to the case of an e^+e^- collider, where the cross section depends only on $\cos^2\theta_{\tilde{t}}$ [10]. Note that the Higgs boson contribution can be larger than the gauge boson contribution. This is in particular the case for large mixing in the top squark sector because the Higgs boson couples more strongly to the left–right combination of the top squarks than to the left-left or right-right combinations. The Higgs boson contribution vanishes for $\cos\theta_{\tilde{t}}\simeq -0.25$ because the corresponding coupling is zero for the parameters chosen. One can disentangle the Higgs boson contribution from the gauge boson part by measuring the differential cross section. As can be seen in Eq. (9), the Higgs boson contribution of the differential cross section does not depend on ϑ whereas the gauge boson contribution shows a $\sin^2\vartheta$ shape. We can safely neglect the interference terms between gauge and Higgs bosons because they are rather small as we have seen above. In Fig. 3b the total cross section is shown for various values of $\sqrt{s}$ between 444 GeV and 454 GeV. For larger values of $\sqrt{s}$, the cross section is decreasing because m_{H^0} varies between 452.8 GeV ($\cos\theta_{\tilde{t}}\sim 0.71$) and 454.2 GeV ($\cos\theta_{\tilde{t}}\sim -0.71$). The $\cos\theta_{\tilde{t}}$ dependence of m_{H^0} is also the reason for $\sigma(\sqrt{s}=454)>(<)\sigma(\sqrt{s}=453)$ if $\cos\theta_{\tilde{t}}<(>)-0.25$.

In Fig. 3c we show $\sigma(\mu^+\mu^-\to\tilde{t}_1\bar{\tilde{t}}_2)$, the Higgs boson contribution and the gauge boson contribution as a function of $\cos\theta_{\tilde{t}}$. An interesting feature here is that for $\cos\theta_{\tilde{t}}=0$ only the Higgs bosons contribute. Moreover, the contribution

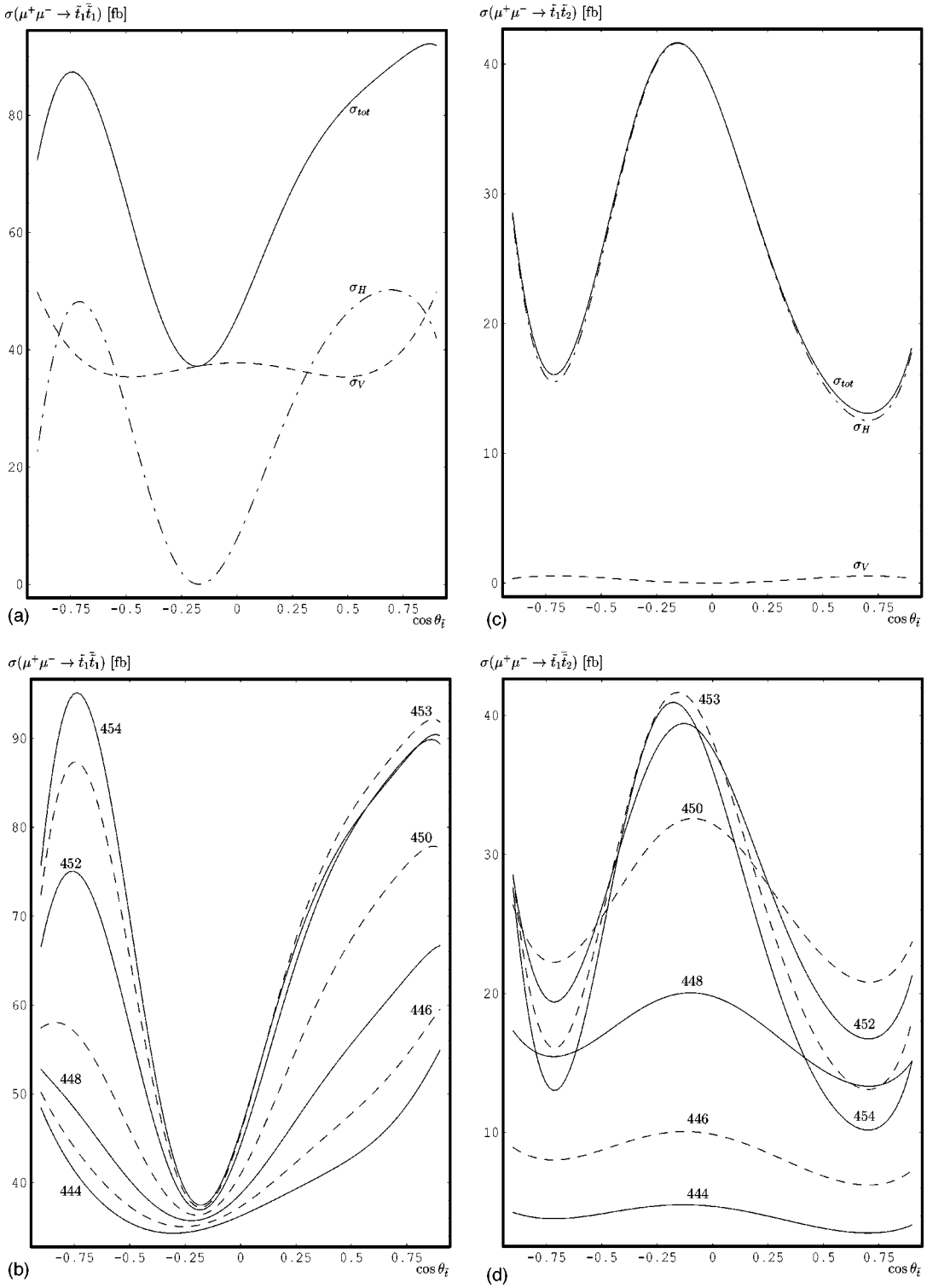

FIG. 3. Cross sections for stop production as a function of $\cos\theta_{\tilde{t}}$ for $m_{\tilde{t}_1}=180$ GeV, $m_{\tilde{t}_2}=260$ GeV, $A_b=300$ GeV, $\mu=300$ GeV, $M=120$ GeV, $\tan\beta=3$, and $m_{A^0}=450$ GeV. In (a) and (c) $\sqrt{s}=453$ GeV and the graphs correspond to: total cross section σ_{tot} (full line), Higgs boson contribution σ_H (dashed-dotted line), and gauge boson contribution σ_V (dashed line). In (b) and (d) the cross section is shown for various $\sqrt{s}$ values (in GeV): 444, 448, 452, 454 (full lines) and 446, 450, 453 (dashed lines).

of the Higgs bosons H_0 and A_0 is generally larger than that of the gauge boson. The total cross section again depends on the sign of $\cos\theta_{\tilde{t}}$. In Fig. 3d we show the total cross section for various values of $\sqrt{s}$. The shift of the peak is due the dependence of m_{H^0} and $\cos\alpha$ on A_t which is calculated from $\cos\theta_{\tilde{t}}$. Note that the coupling $H^0\tilde{t}_1\tilde{t}_2$ is large in the range where the coupling $H^0\tilde{t}_1\tilde{t}_1$ is small and vice versa. The minima near $|\cos\theta_{\tilde{t}}|\simeq 0.71$ are due to the vanishing of the coupling $H^0\tilde{t}_1\tilde{t}_2$.

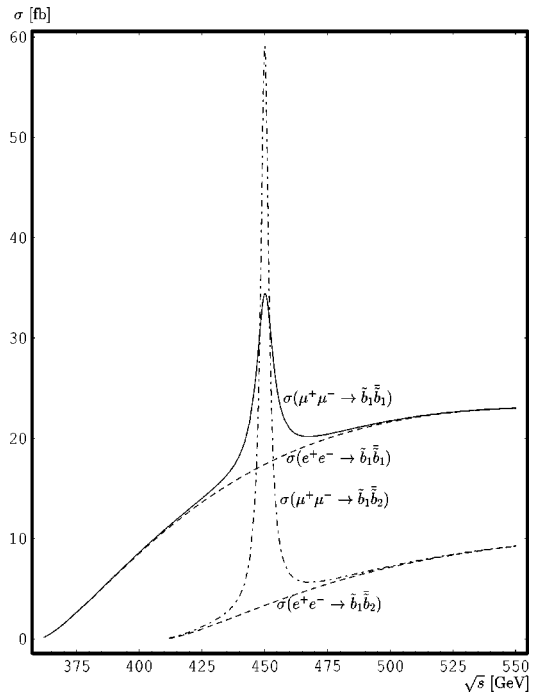

FIG. 4. Cross sections for sbottom production as a function of $\sqrt{s}$ for $m_{\tilde{b}_1}=180$ GeV, $m_{\tilde{b}_2}=230$ GeV, $\cos\theta_{\tilde{b}}=0.755$, $m_{\tilde{t}_1}=160$ GeV, $m_{\tilde{t}_2}=300$ GeV, $\cos\theta_{\tilde{t}}=0.615$, $\mu=291$ GeV, $M=120$ GeV, $\tan\beta=8$, and $m_{A^0}=450$ GeV.

In Fig. 4 the cross sections for sbottom production are shown as a function of $\sqrt{s}$ for $m_{\tilde{b}_1}=180$ GeV, $m_{\tilde{b}_2}=230$ GeV, $\cos\theta_{\tilde{b}}=0.755$, $m_{\tilde{t}_1}=160$ GeV, $m_{\tilde{t}_2}=300$ GeV, $\cos\theta_{\tilde{t}}=0.615$, $\mu=291$ GeV, $\tan\beta=8$, and $m_{A^0}=450$ GeV. $M_{\tilde{L}}$, $M_{\tilde{E}}$, and A_τ are taken as above. It is interesting that $\sigma(\mu^+\mu^-\to\tilde{b}_1\bar{\tilde{b}}_2)$ is ~ 20 times larger than $\sigma(e^+e^-\to\tilde{b}_1\bar{\tilde{b}}_2)$ at $\sqrt{s}=m_{A^0}$. This has two implications: First, one gets a cross section that is large enough to be measured even with an integrated luminosity of 10 fb^{-1}. Second, the $b_1\bar{\tilde{b}}_2$ cross section is even larger than the $\tilde{b}_1\bar{\tilde{b}}_1$ production cross section. Note that we only show the cross section for $b_1\bar{\tilde{b}}_2$ whereas in the experiment one can measure the cross section of $\tilde{b}_1\bar{\tilde{b}}_2+\bar{\tilde{b}}_1\tilde{b}_2$.

In Fig. 5 we show the cross sections for sbottom production as a function of $\cos\theta_{\tilde{b}}$ for $m_{\tilde{b}_1}=180$ GeV, $m_{\tilde{b}_2}=230$ GeV, $A_b=300$ GeV, $m_{\tilde{t}_1}=160$ GeV, $m_{\tilde{t}_2}=300$ GeV, $\tan\beta=8$, and $m_{A^0}=450$ GeV. $M_{\tilde{L}}$, $M_{\tilde{E}}$, and A_τ are taken as above. We have calculated the other parameters in the following way: From $m_{\tilde{b}_1}, m_{\tilde{b}_2}, \cos\theta_{\tilde{b}}$, and A_b we get $M_{\tilde{Q}}$, $M_{\tilde{D}}$, and μ. We then take $M_{\tilde{Q}}$, $m_{\tilde{t}_1}$, and $m_{\tilde{t}_2}$ to calculate $M_{\tilde{U}}$, $\cos\theta_{\tilde{t}}$, and A_t. There are similarities to the stop case: For $\tilde{b}_1\bar{\tilde{b}}_1$ production the Higgs boson contribution can be larger than the gauge boson part (Fig. 5a). In the case of $\tilde{b}_1\bar{\tilde{b}}_2$ production, the contribution of the Higgs bosons is much larger than that of the gauge boson (Fig. 5c). The main difference compared to the stop case is that the asymmetry in the sign of $\cos\theta_{\tilde{b}}$ is much more pronounced in the $\tilde{b}_1\bar{\tilde{b}}_2$ channel than in the $\tilde{b}_1\bar{\tilde{b}}_1$ channel as a consequence of the corresponding couplings (Fig. 5b and d). The peak at $\cos\theta_{\tilde{b}}\simeq 0.71$ in Fig. 5d results not only from the couplings, but also from the fact that the total decay width of A^0 has a minimum there.

In Fig. 6 the stau production cross sections are shown as a function of $\sqrt{s}$ for $m_{\tilde{\tau}_1}=90$ GeV, $m_{\tilde{\tau}_2}=127$ GeV, $\cos\theta_{\tilde{\tau}}=0.594$, $M_{\tilde{Q}}=300$ GeV, $M_{\tilde{U}}=270$ GeV, $M_{\tilde{D}}=330$ GeV, $A_t=A_b=350$ GeV, $\mu=300$ GeV, $\tan\beta=8$, and $m_{A^0}=220$ GeV. The parameters are chosen such that the Higgs boson cannot decay into squarks or the top quark. Therefore, the total decay widths of H^0 and A^0 are one order of magnitude smaller than in the previous examples. This leads to the large peaks at $\sqrt{s}=m_{A^0}, m_{H^0}$. Moreover, the decay widths are so small that one can see two peaks in the case of $\tilde{\tau}_1\bar{\tilde{\tau}}_2$ production. It should be possible to observe both peaks in a real experiment because of the good energy resolution of a $\mu^+\mu^-$ collider [6].

In Fig. 7 the cross sections for stau production are presented as a function of $\cos\theta_{\tilde{\tau}}$ for $m_{\tilde{\tau}_1}=90$ GeV, $m_{\tilde{\tau}_2}=127$ GeV, $A_\tau=300$ GeV. $\tan\beta$, m_{A^0}, and the squark parameters are taken as above. We have calculated $M_{\tilde{L}}$, ME, and μ from $m_{\tilde{\tau}_{1,2}}$ and $\cos\theta_{\tilde{\tau}}$. With these and the other parameters, we have calculated $m_{\tilde{\nu}_\tau}$, m_{H^0}, $\cos\alpha$, Γ_{H^0}, and Γ_{A^0}. Note that the masses, mixing angle, and decay widths of the Higgs bosons depend indirectly on $\cos\theta_{\tilde{\tau}}$ due to the induced change in μ. This fact leads to the observed shifts of the maximal cross section with $\sqrt{s}$ in Fig. 7b and d. In $\tilde{\tau}_1\bar{\tilde{\tau}}_2$ production the Higgs boson contribution is much larger than the gauge boson contribution (Fig. 7c) similar to the squark production. This is particularly important, because in this case the production cross section is most likely too small to be seen at an e^+e^- collider [10,11]. The cross sections depend strongly on the sign of $\cos\theta_{\tilde{\tau}}$ in both channels (Fig. 7a and c). Note also that, for the parameters chosen in the Higgs couplings to the staus, the gauge couplings are of the same size as the Yukawa couplings [Eqs. (A10)–(A12)]:

In Fig. 8 we show the total cross sections for sneutrino production as a function of $\sqrt{s}$ for the same parameters as in Fig. 6 (implying $m_{\tilde{\nu}_\tau}=83.6$ GeV). The large peak at $\sqrt{s}=m_{H^0}$ is due to the small total decay width of H^0 ($\Gamma_{H^0}\simeq 0.8$ GeV) and due to the coupling $H^0\tilde{\nu}_\tau\tilde{\nu}_\tau$ which is a gauge coupling [see Eq. (A9)] stemming from a D term.

IV. SUMMARY

We have studied sfermion pair production in $\mu^+\mu^-$ annihilation focusing on the impact of the Higgs boson resonances in these processes. We have seen that the production cross sections can be considerably enhanced at these resonances for all sfermions of the third generation. The most important results are: First, the production cross sections depend on the sign of $\cos\theta_{\tilde{f}}$. Second, the Higgs boson contributions dominate the production cross section of $\tilde{f}_1\bar{\tilde{f}}_2$. We have seen that the cross sections can be large enough to be studied at a $\mu^+\mu^-$ collider even if the corresponding cross

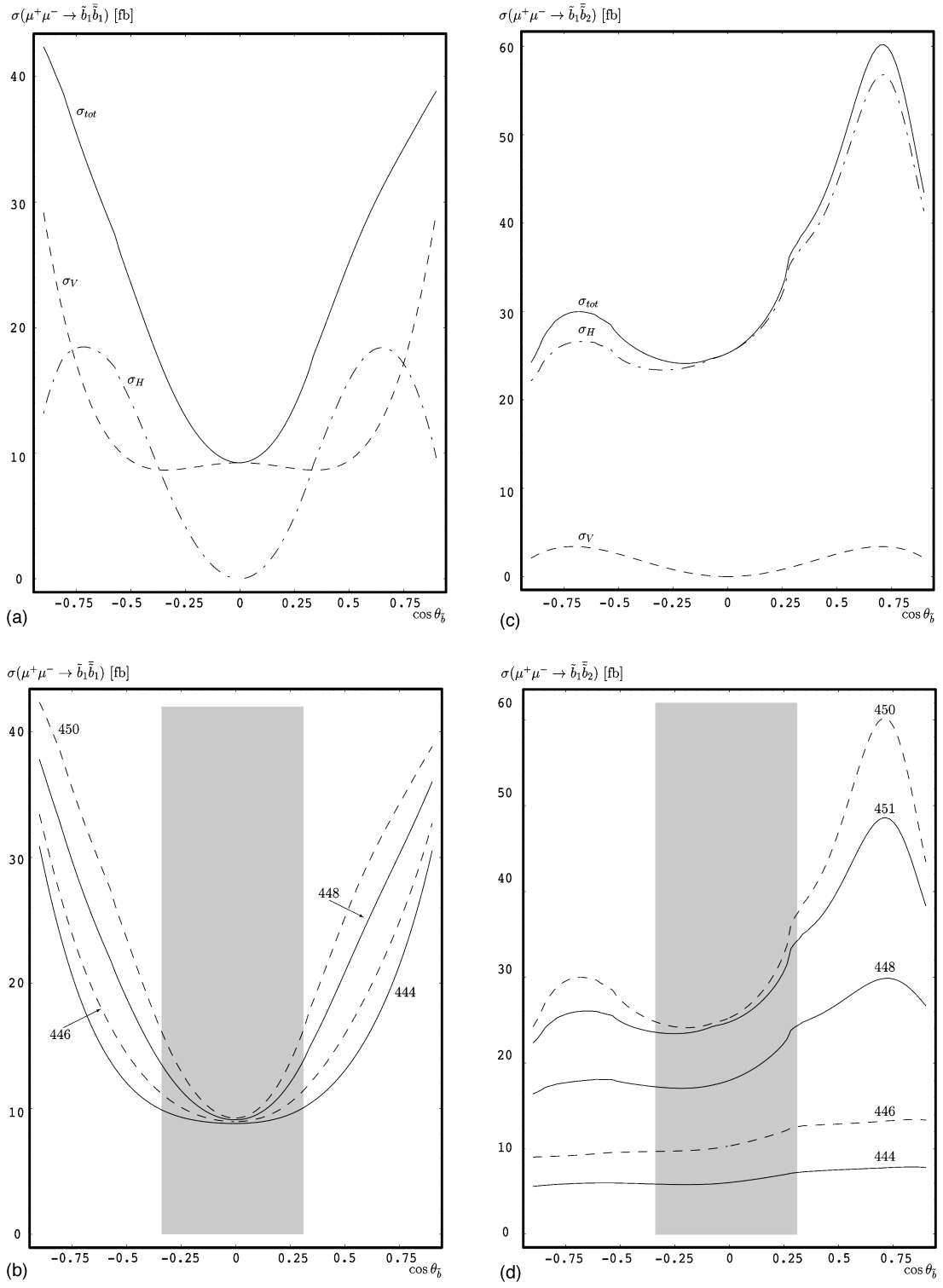

FIG. 5. Cross sections for sbottom production as a function of $\cos\theta_{\tilde{b}}$ for $m_{\tilde{b}_1}=180$ GeV, $m_{\tilde{b}_2}=230$ GeV, $A_b=300$ GeV, $m_{\tilde{t}_1}=160$ GeV, $m_{\tilde{t}_2}=300$ GeV, $M=120$ GeV, $\tan\beta=8$, and $m_{A^0}=450$ GeV. In (a) and (c) $\sqrt{s}=450$ GeV and the graphs correspond to: total cross section σ_{tot} (full line), Higgs boson contribution σ_H (dashed-dotted line), and gauge boson contribution σ_V (dashed line). In (b) and (d) the cross section is shown for various $\sqrt{s}$ values (in GeV): 444, 448, 451 (full lines) and 446, 450 (dashed lines). The gray area is excluded by LEP2 ($m_{\tilde{\chi}_1^+}<90$ GeV).

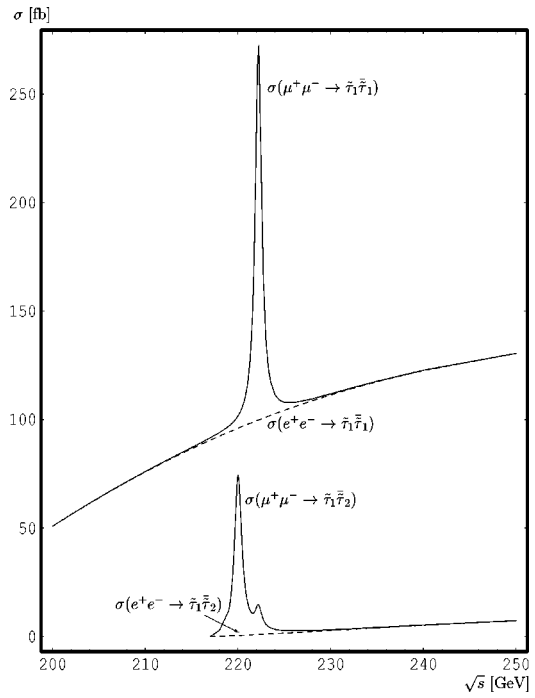

FIG. 6. Cross sections for stau production as a function of $\sqrt{s}$ for $m_{\tilde{\tau}_1}=90$ GeV, $m_{\tilde{\tau}_2}=127$ GeV, $\cos\theta_{\tilde{\tau}}=0.594$, $M_{\tilde{Q}}=300$ GeV, $M_{\tilde{U}}=270$ GeV, $M_{\tilde{D}}=330$ GeV, $A_t=350$ GeV, $A_b=350$ GeV, $\mu=300$ GeV, $M=120$ GeV, $\tan\beta=8$, and $m_{A^0}=220$ GeV. The full lines show the cross sections at a $\mu^+\mu^-$ collider and the dashed lines the corresponding ones at an e^+e^- collider.

sections are too small to be measured at an e^+e^- collider. Third, the Higgs boson contribution can even be larger than the gauge boson contributions in the $\tilde{f}_1\bar{\tilde{f}}_1$ channel. From these facts we conclude that a $\mu^+\mu^-$ collider is an excellent machine for obtaining important information on the $H^0\tilde{f}_i\tilde{f}_j$ and $A^0\tilde{f}_1\tilde{f}_2$ couplings.

ACKNOWLEDGMENTS

We are very grateful to M. Carena and S. Protopopescu for their kind invitation to the ''Workshop on Physics at the First Muon Collider, and the Front End of a Muon Collider,'' Batavia, Illinois, where this study was initiated. This work was supported by the ''Fonds zur Förderung der wissenschaftlichen Forschung'' of Austria, project No. P10843–PHY.

APPENDIX A: HIGGS COUPLINGS

In this section we list the couplings of the neutral Higgs bosons to sfermions. We concentrate here on the couplings of H^0 and A^0 which are important for our investigation. One can get the couplings of h^0 from those of H^0 by the replacements: $\cos\alpha\rightarrow-\sin\alpha$ and $\sin\alpha\rightarrow\cos\alpha$.

Higgs couplings to top squarks:

$$G_{11}^{H^0}=-\frac{m_Z\cos(\alpha+\beta)}{4\cos\theta_W}-\frac{m_Z}{2\cos\theta_W}\left(\frac{1}{2}-\frac{4}{3}\sin^2\theta_W\right)\times\cos(\alpha+\beta)\cos2\theta_{\tilde{t}}-\frac{m_t^2\sin\alpha}{m_W\sin\beta}+\frac{m_t}{2m_W\sin\beta}\times(\mu\cos\alpha-A_t\sin\alpha)\sin2\theta_{\tilde{t}}, \tag{A1}$$

$$G_{12}^{H^0}=\frac{m_Z}{2\cos\theta_W}\left(\frac{1}{2}-\frac{4}{3}\sin^2\theta_W\right)\cos(\alpha+\beta)\sin2\theta_{\tilde{t}}+\frac{m_t}{2m_W\sin\beta}(\mu\cos\alpha-A_t\sin\alpha)\cos2\theta_{\tilde{t}}, \tag{A2}$$

$$G_{22}^{H^0}=-\frac{m_Z\cos(\alpha+\beta)}{4\cos\theta_W}+\frac{m_Z}{2\cos\theta_W}\left(\frac{1}{2}-\frac{4}{3}\sin^2\theta_W\right)\times\cos(\alpha+\beta)\cos2\theta_{\tilde{t}}-\frac{m_t^2\sin\alpha}{m_W\sin\beta}-\frac{m_t}{2m_W\sin\beta}\times(\mu\cos\alpha-A_t\sin\alpha)\sin2\theta_{\tilde{t}}, \tag{A3}$$

$$G_{12}^{A^0}=-G_{21}^{A^0}=\frac{m_t}{2m_W}(A_t\cot\beta+\mu). \tag{A4}$$

Higgs couplings to sbottoms:

$$G_{11}^{H^0}=-\frac{m_Z\cos(\alpha+\beta)}{4\cos\theta_W}-\frac{m_Z}{2\cos\theta_W}\left(-\frac{1}{2}+\frac{2}{3}\sin^2\theta_W\right)\times\cos(\alpha+\beta)\cos2\theta_{\tilde{b}}-\frac{m_b^2\cos\alpha}{m_W\cos\beta}+\frac{m_b}{2m_W\cos\beta}\times(\mu\sin\alpha-A_b\cos\alpha)\sin2\theta_{\tilde{b}}, \tag{A5}$$

$$G_{12}^{H^0}=\frac{m_Z}{2\cos\theta_W}\left(-\frac{1}{2}+\frac{2}{3}\sin^2\theta_W\right)\cos(\alpha+\beta)\sin2\theta_{\tilde{b}}+\frac{m_b}{2m_W\cos\beta}(\mu\sin\alpha-A_b\cos\alpha)\cos2\theta_{\tilde{b}}, \tag{A6}$$

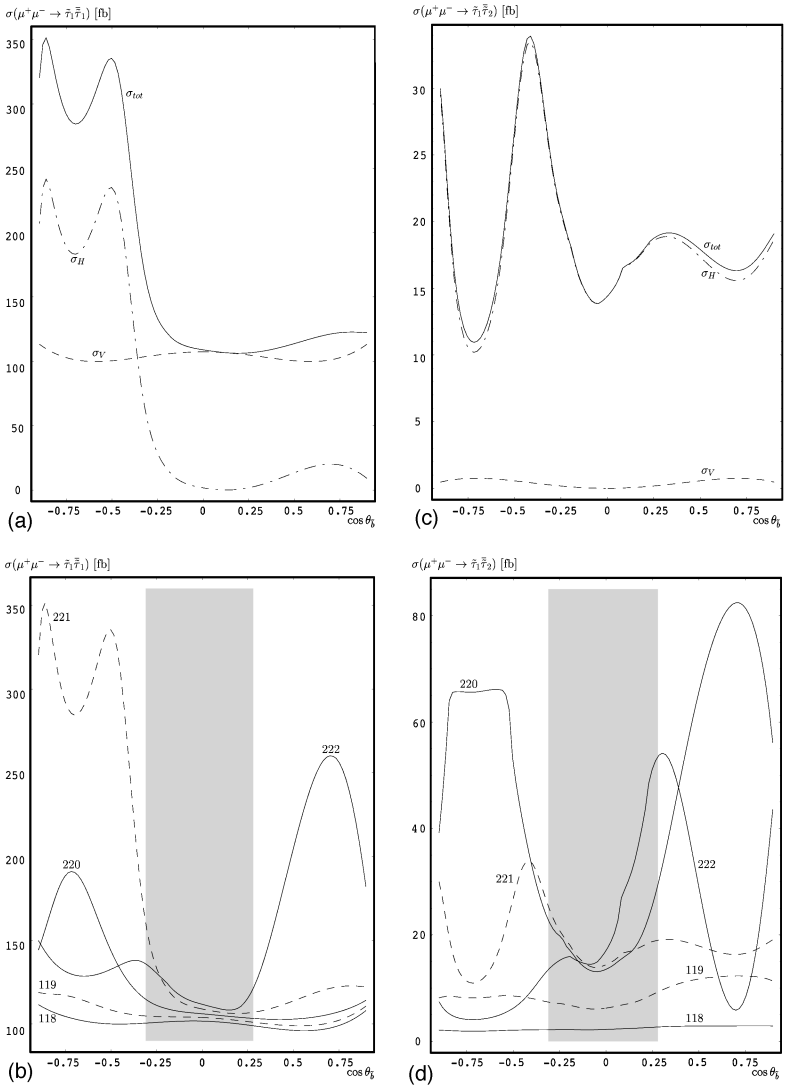

FIG. 7. Cross sections for $\tilde{\tau}$ production as a function of $\cos\theta_{\tilde{\tau}}$ for $m_{\tilde{\tau}_1}=90$ GeV, $m_{\tilde{\tau}_2}=127$ GeV, $A_\tau=300$ GeV, $M=120$ GeV, $\tan\beta=8$, and $m_{A^0}=220$ GeV. In (a) and (c) $\sqrt{s}=221$ GeV and the graphs correspond to: total cross section σ_{tot} (full line), Higgs boson contribution σ_H (dashed-dotted line), and gauge boson contribution σ_V (dashed line). In (b) and (d) the cross section is shown for various $\sqrt{s}$ values (in GeV): 218, 220, 222 (full lines) and 219, 221 (dashed lines). The gray area is excluded by LEP2 ($m_{\tilde{\chi}_1^+}<90$ GeV).

$$G_{22}^{H^0}=-\frac{m_Z\cos(\alpha+\beta)}{4\cos\theta_W}+\frac{m_Z}{2\cos\theta_W}\left(-\frac{1}{2}+\frac{2}{3}\sin^2\theta_W\right)$$

$$\times\cos(\alpha+\beta)\cos2\theta_{\tilde{b}}-\frac{m_b^2\cos\alpha}{m_W\cos\beta}-\frac{m_b}{2m_W\cos\beta}$$

$$\times(\mu\sin\alpha-A_b\cos\alpha)\sin2\theta_{\tilde{b}}, \tag{A7}$$

$$G_{12}^{A^0}=-G_{21}^{A^0}=\frac{m_b}{2m_W}(A_b\tan\beta+\mu). \tag{A8}$$

Higgs coupling to the tau-sneutrino:

$$G_{11}^{H^0}=-\frac{m_Z\cos(\alpha+\beta)}{2\cos\theta_W}. \tag{A9}$$

Higgs couplings to staus:

$$G_{11}^{H^0}=-\frac{m_Z\cos(\alpha+\beta)}{4\cos\theta_W}-\frac{m_Z}{2\cos\theta_W}\left(-\frac{1}{2}+\sin^2\theta_W\right)$$

$$\times\cos(\alpha+\beta)\cos2\theta_{\tilde{\tau}}-\frac{m_\tau^2\cos\alpha}{m_W\cos\beta}+\frac{m_\tau}{2m_W\cos\beta}$$

$$\times(\mu\sin\alpha-A_\tau\cos\alpha)\sin2\theta_{\tilde{\tau}}, \tag{A10}$$

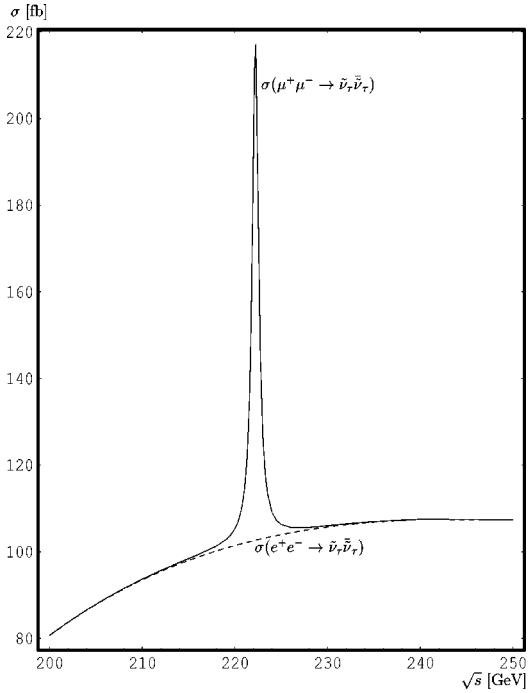

FIG. 8. Cross sections for sneutrino production as a function of $\sqrt{s}$ for $m_{\tilde{\nu}_\tau}=83.6\,\mathrm{GeV}$ and the other parameters as in Fig. 6. The full line shows the cross sections at a $\mu^+\mu^-$ collider and the dashed line the corresponding one at an e^+e^- collider.

$$G_{12}^{H^0}=\frac{m_Z}{2\cos\theta_W}\left(-\frac{1}{2}+\sin^2\theta_W\right)\cos(\alpha+\beta)\sin2\theta_\tau^{\sim}$$

$$+\frac{m_\tau}{2m_W\cos\beta}(\mu\sin\alpha-A_\tau\cos\alpha)\cos2\theta_\tau^{\sim}, \qquad \text{(A11)}$$

$$G_{22}^{H^0}=-\frac{m_Z\cos(\alpha+\beta)}{4\cos\theta_W}+\frac{m_Z}{2\cos\theta_W}\left(-\frac{1}{2}+\sin^2\theta_W\right)$$

$$\times\cos(\alpha+\beta)\cos2\theta_\tau^{\sim}-\frac{m_\tau^2\cos\alpha}{m_W\cos\beta}-\frac{m_\tau}{2m_W\cos\beta}$$

$$\times(\mu\sin\alpha-A_\tau\cos\alpha)\sin2\theta_\tau^{\sim}, \qquad \text{(A12)}$$

$$G_{12}^{A^0}=-G_{21}^{A^0}=\frac{m_\tau}{2m_W}(A_\tau\tan\beta+\mu). \qquad \text{(A13)}$$

[1] H. P. Nilles, Phys. Rep. **110**, 1 (1984).

[2] H. E. Haber and G. L. Kane, Phys. Rep. **117**, 75 (1985).

[3] I. Hinchliffe *et al.*, Phys. Rev. D **55**, 5520 (1997); F. Paige, in Proceedings of the ''Workshop on Physics at the First Muon Collider and at the Front End of a Muon Collider,'' Batavia, Illinois, 1997, hep-ph/9801395.

[4] J. F. Gunion, in Proceedings of ''Workshop on Physics at the First Muon Collider and at the Front End of the Muon Collider,'' Batavia, Illinois, 1997, hep-ph/9802258.

[5] J. F. Gunion *et al.*, Proceedings of the 1996 DPF/DPB Summer Study on High-Energy Physics, Snowmass, Colorado, 1996, edited by D. G. Cassel, L. Trindle Gennari, and R. H. Siemann (SLAC, Menlo Park, CA, 1997), Vol. 2, p. 541.

[6] V. Barger, M. S. Berger, J. F. Gunion, and T. Han, Phys. Rep. **286**, 1 (1997); H. E. Haber, talk given at the ''Workshop on Physics at the First Muon Collider and at the Front End of the Muon Collider,'' Batavia, Illinois.

[7] J. F. Gunion and H. E. Haber, Nucl. Phys. **B272**, 1 (1986).

[8] J. F. Gunion, H. E. Haber, G. L. Kane, and S. Dawson, *The Higgs Hunter's Guide* (Addison-Wesley, Reading, MA, 1990), and references therein.

[9] J. Ellis and S. Rudaz, Phys. Lett. **128B**, 248 (1983); G. Altarelli and R. Rückl, *ibid.* **144B**, 126 (1984).

[10] A. Bartl, W. Majerotto, and W. Porod, Z. Phys. C **64**, 499 (1994); A. Bartl *et al.*, *ibid.* **73**, 469 (1997); **76**, 549 (1997).

[11] ECFA/DESY LC Physics Working Group, E. Accomando *et al.*, Phys. Rep. **299**, 1 (1998).

[12] J. Ellis, G. Ridolfi, and F. Zwirner, Phys. Lett. B **257**, 83 (1991); **262**, 477 (1991).

[13] H. E. Haber and R. Hempfling, Phys. Rev. Lett. **66**, 1815 (1991).

[14] L. E. Ibáñez and G. G. Ross, Phys. Lett. **110B**, 215 (1982).

[15] H. Eberl, A. Bartl, and W. Majerotto, Nucl. Phys. **B472**, 481 (1996).

[16] A. Bartl, H. Eberl, K. Hidaka, T. Kon, W. Majerotto, and Y. Yamada, Phys. Lett. B **389**, 538 (1996).

[17] A. Bartl, H. Eberl, K. Hidaka, T. Kon, W. Majerotto, and Y. Yamada, Phys. Lett. B **402**, 303 (1997).

[18] A. Djouadi, J. Kalinowski, P. Ohmann, and P. M. Zerwas, Z. Phys. C **74**, 93 (1997).